Coexistence of principal and tilted axis rotation in ^{110}Ag

B. Das,[1] P. Datta,[2,*] S. Chattopadhyay,[1] S. Roy,[3,4] R. Raut,[5] R. K. Bhowmik,[6] A. Goswami,[1] H. C. Jain,[7] R. Kumar,[6] S. Muralithar,[6] D. Negi,[8] S. Pal,[8] R. Palit,[7] and R. P. Singh[6]

[1]*Saha Institute of Nuclear Physics, HBNI, Kolkata 700064, India*
[2]*Ananda Mohan College, Kolkata 700009, India*
[3]*Ronin Institute, 127 Haddon Pl. Montclair, New Jersey 07043-2314, USA*
[4]*Institute for Globally Distributed Open Research and Education, Dal 120, 311 65 Vessigebro, Sweden*
[5]*UGC-DAE Consortium for Scientific Research, Kolkata Centre, Kolkata 700098, India*
[6]*Inter University Accelerator Center, New Delhi 110067, India*
[7]*Tata Institute of Fundamental Research, Mumbai 400005, India*
[8]*Centre for Excellence in Basic Sciences, Mumbai 400098, India*

(Received 28 April 2018; published 27 July 2018)

The positive-parity band structure of ^{110}Ag has been established for the first time. A new decay path to the isomeric 6^+ state has been observed for this band. The lifetimes of the high spin levels have been measured using the Doppler-shift attenuation method. The comparison of the experimental data with the numerical results of the shears mechanism with principal axis cranking calculation indicates that this band originates due to the tilted axis rotation. On the other hand, it has already been established that the negative-parity levels in the same spin domain originate due to the principal axis rotation.

DOI: 10.1103/PhysRevC.98.014326

I. INTRODUCTION

The Ag isotopes are in the focus of contemporary nuclear structure research in connection to the observation of nearly degenerate bands and the possibility of identifying them as chiral partners. These experimental studies are primarily centered around the negative-parity doublet bands with $\pi g_{9/2}^{-1} \otimes \nu h_{11/2}^{1}$ configuration [1–4]. The results seem to indicate that these doublet bands may correspond to different nuclear shapes associated with different γ values and are not the chiral partners [4]. This is not uncommon among nuclei to possess large γ softness where the valance neutrons and the protons occupy competing shape-driving orbitals and the Ag isotopes are no exceptions. However, such configurations may also lead to shearslike structures [5–8], and hence, the tilted (nonprincipal) axis rotation emerges as an alternate possibility of generating the higher angular momentum states. Such possibilities have been investigated in Ag isotopes both for the positive and the negative-parity bands up to ^{109}Ag [7–10]. It has been observed that for the higher spin states, the in-band $M1$ transition energies exhibit an increasing trend while the $B(M1)$ transitions rates fall smoothly with increasing spin. These features indicate the loss of π-rotational symmetry as a consequence of tilted axis rotation [6]. However, it is to be noted that these transitional nuclei are moderately deformed, therefore, the role of core rotation needs to be considered. This is corroborated by the fact that the majority of these bands are observed beyond the maximum spin achievable by the complete closing of the angular momentum vectors of the valance quasiparticles as described in the shears model [11]. Thus, a semiclassical model, shears with principal axis cranking (SPAC) [12], has been successfully employed in recent times to study both the positive and the negative-parity bands of the Ag isotopes [9,10].

A deviation from this systematic was first reported by our group in ^{110}Ag [13]. It is the heaviest Ag isotope studied so far using the heavy-ion-induced fusion evaporation reaction and only the negative-parity yrast band was established. Unlike the lighter Ag isotopes, the high spin states of ^{110}Ag display staggering of the in-band $M1$ transition energies and in the $B(M1)$ transition rates, till the highest observed spin of $20\hbar$ [13]. This observed staggering is the characteristic of the principal axis rotation and is associated with the signature quantum number. Thus, $N = 62$ is the neutron boundary for the dominance of the tilted axis rotation along the yrast band in Ag isotopes. However, it is an open question whether the same conclusion holds true for the non-yrast bands of ^{110}Ag.

In this work, a non-yrast positive-parity band has been identified for the first time, which predominantly decays to the isomeric 6^+ state through a newly observed decay path and also through the known yrast sequence [13]. The level lifetime measurements have been carried out in this band and the extracted transition rates have been compared with the SPAC numerical calculations to understand the underlying angular momentum generation mechanism.

II. EXPERIMENT

The high spin states of ^{110}Ag were populated using the 70 MeV ^{18}O beam from the 15-UD Pelletron at Inter University Accelerator Center, New Delhi through the ^{96}Zr

*Corresponding author: pdatta.ehp@gmail.com

(^{18}O, $p3n$)^{110}Ag reaction. The 1 mg/cm^2 thick enriched ^{96}Zr target had a ^{206}Pb backing of thickness 9 mg/cm^2. The γ rays were detected in the Indian National Gamma Array (INGA) [14], which consisted of 18 Compton suppressed clover detectors. These detectors were arranged in rings at 32°, 57°, 90°, 123°, and 148° with respect to the beam direction. The target to detector distance was 25 cm. The data trigger was set to threefold or higher prompt γ-ray coincidence, which resulted into 1.3×10^9 events. It is to be noted that the ^{96}Zr(^{18}O, $p3n$)^{110}Ag reaction channel contains only about 2% of the total fusion-evaporation cross section while the pure neutron evaporation channels consume 95%. Thus, the present investigation of ^{110}Ag is primarily based on the γ-γ coincidence matrices and the γ-γ-γ cube analysis.

III. ANALYSIS AND RESULTS

The data were sorted into the matrices and the cube using the sorting codes INGASORT [15] and SPRINGZ [16] developed at Inter University Accelerator Center, New Delhi and UGC-DAE Consortium for Scientific Research, Kolkata, respectively. The further analysis was done using the RADWARE programs, GTKESC and GTKLEV [17]. The angle-dependent asymmetric matrices were used for the line-shape analysis using the Doppler-shift attenuation method (DSAM). In order to measure the γ-ray multipolarities by the directional correlations from oriented states (DCO) ratio method [18], an angle-dependent matrix was constructed by placing the γ-ray energy detected at 90° along one axis while the coincident γ-ray energy at 32° on the other axis. The linear polarization measurement was also performed to extract the electromagnetic character of the deexciting γ rays using the integrated polarization from directional correlation of oriented states method (iPDCO) [19]. The details of the method and the procedure have been discussed in Ref. [7]. These analysis were first performed on the strong transitions of the ^{109}Cd and validated.

The non-yrast levels of ^{110}Ag were first identified using the 1357 keV gate (shown in the inset of Fig. 1), which showed a sequence of low-energy γ transitions (185, 194, 246, and 320 keV) in coincidence with the 191, 407, and 746 keV transitions of the yrast cascade. The observation of the crossover transitions corresponding to these transitions confirm their placement, and their $\Delta I = 1$ character. The other γ rays deexciting the positive-parity levels of ^{110}Ag were identified from the triple gate of 273 ($7^+ \rightarrow 6^+$) or 384 ($8^+ \rightarrow 7^+$) keV and 194 ($14^+ \rightarrow 13^+$) or 246 ($15^+ \rightarrow 14^+$) keV as shown in Fig. 1. These newly observed transitions were placed according to their relative intensities after satisfying the corresponding coincidence criteria. The result of these observations has been summarized in the partial level scheme of ^{110}Ag as shown in Fig. 2. It is to be noted that few positive-parity states were previously reported [20]. However, these states were not observed in the present experiment.

In order to measure the relative intensities of the positive-parity states, the intensities of the 194 and 246 keV transitions were first estimated from the 191 ($9^- \rightarrow 8^-$) keV gate and were normalized with respect to the intensities of the 468 ($14^- \rightarrow 13^-$) and 491 ($13^- \rightarrow 12^-$) keV. These normalized values were further multiplied by the intensity ratio of 273 to 191 keV transitions extracted from the 194 and 246 keV triple gate to estimate the true intensities of the 194 and 246 keV transitions. The further increment to the intensities due to the

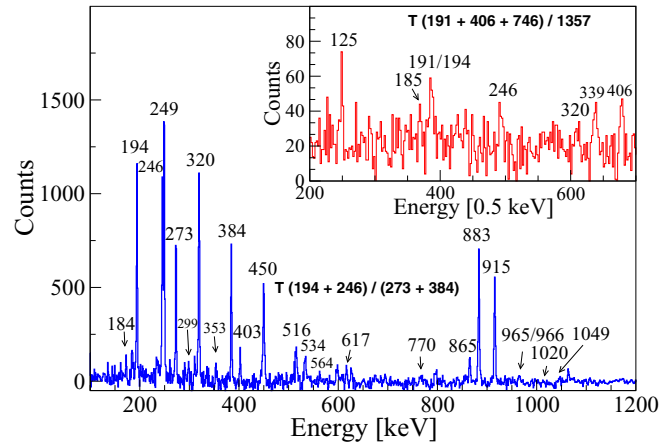

FIG. 1. The triples gated spectrum generated by the coincidence condition of 194 ($14^+ \rightarrow 13^+$) or 246 ($15^+ \rightarrow 14^+$) keV with 273 ($7^+ \rightarrow 6^+$) or 384 ($8^+ \rightarrow 7^+$) keV transitions. The transitions belonging to the positive-parity band of ^{110}Ag are marked accordingly. The triples spectrum of 1357 ($12^+ \rightarrow 11^-$) keV transition with 191 ($9^- \rightarrow 8^-$) or 407($10^- \rightarrow 9^-$) or 746 ($11^- \rightarrow 9^-$) keV transitions is shown in the inset.

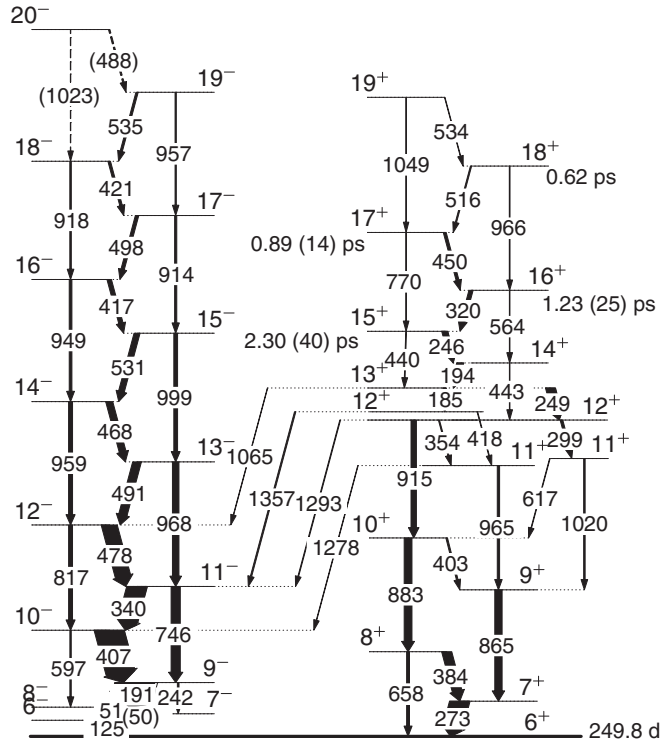

FIG. 2. The partial level scheme of the ^{110}Ag. All the excited positive-parity states and its decay paths have been observed for the first time. The deduced level lifetimes for the 15^+, 16^+, 17^+, and 18^+ levels are indicated. However, the quoted value for the 18^+ level is the effective lifetime.

TABLE I. The energies, the relative intensities, the DCO and the iPDCO ratios for γ transitions in between the positive-parity levels of ^{110}Ag. The uncertainty in the γ-ray energies were ~ 0.4 keV for strong transitions (intensity $\geqslant 10$) and ~ 0.6 keV for weaker transitions. The DCO ratios were measured from the gated spectra of 194 or 249 keV gating transitions, where the values using the second gate is indexed with superscript a. The relative intensities were scaled by considering the intensity of 191 ($9^- \rightarrow 8^-$) keV transition as 100.

E_γ(keV)	$I_i^\pi \rightarrow I_f^\pi$	Rel. Intensity	DCO	iPDCO
185	$13^+ \rightarrow 12^+$	7.8(1.0)	0.77(0.20)	
194	$14^+ \rightarrow 13^+$	16.6(1.1)	0.82(0.12)^a	
246	$15^+ \rightarrow 14^+$	14.7(1.0)	0.92(0.12)	
249	$13^+ \rightarrow 12^+$	24.3(0.9)	1.07(0.13)	−0.02(0.01)
273	$7^+ \rightarrow 6^+$	50.0(3.0)	0.69(0.11)	
299	$12^+ \rightarrow 11^+$	6.5(1.2)	0.84(0.10)^a	
320	$16^+ \rightarrow 15^+$	10.3(1.1)	0.70(0.14)	−0.18(0.10)
354	$12^+ \rightarrow 11^+$	2.7(0.6)		
384	$8^+ \rightarrow 7^+$	25.1(3.0)	0.67(0.14)	−0.08(0.10)
403	$10^+ \rightarrow 9^+$	4.1(0.6)	0.71(0.20)	
418	$12^+ \rightarrow 11^+$	1.5(0.3)	0.79(0.22)	
440	$15^+ \rightarrow 13^+$	1.8(0.3)		
443	$14^+ \rightarrow 13^+$	1.3(0.3)		
450	$17^+ \rightarrow 16^+$	7.3(2.0)		
516	$18^+ \rightarrow 17^+$	3.1(0.8)		
534	$19^+ \rightarrow 18^+$	1.2(0.3)		
564	$16^+ \rightarrow 14^+$	1.4(0.4)		
617	$11^+ \rightarrow 10^+$	1.4(0.2)		
658	$8^+ \rightarrow 6^+$	7.4(1.2)		
770	$17^+ \rightarrow 15^+$	1.3(0.4)		
865	$9^+ \rightarrow 7^+$	18.9(1.5)	1.68(0.71)	0.22(0.08)
883	$10^+ \rightarrow 8^+$	20.1(2.1)		
915	$12^+ \rightarrow 10^+$	13.9(1.6)	1.40(0.25)	0.20(0.09)
965	$11^+ \rightarrow 9^+$	6.0(1.2)	1.20(0.22)^a	0.24(0.08)
966	$18^+ \rightarrow 16^+$	1.8(1.0)		
1020	$11^+ \rightarrow 9^+$	3.8(0.7)		
1049	$19^+ \rightarrow 17^+$	0.7(0.6)		
1065	$13^+ \rightarrow 12^-$	1.0(0.5)		
1278	$11^+ \rightarrow 10^-$	1.1(0.1)	0.76(0.40)	0.15(0.10)
1293	$12^+ \rightarrow 11^-$	1.8(0.2)	0.64(0.14)	
1357	$12^+ \rightarrow 11^-$	3.3(0.2)	0.66(0.20)	0.24(0.13)

parallel decay path of 658 ($8^+ \rightarrow 6^+$) keV was done by noting the relative intensities of 273 and 658 keV transitions. The rest of the γ-ray intensities were determined relative to the estimated intensities of 194 and 246 keV transitions.

It may be noted that the positive-parity band is well anchored with respect to the yrast band through the observation of the four inter-band transitions namely 1065, 1278, 1293, and 1357 keV. Out of these, the DCO and the iPDCO ratios were measured for the 1278 and 1357 keV transitions, which established the $E1$ character for them. This observation was also supported by the fact that both these transitions did not show any line shapes in the angle-dependent matrices. Thus, the spin and the parity of the levels decaying by the 1278 and 1357 keV transitions were fixed to 11^+ and 12^+, respectively. The spins and the parities of the other levels of the positive-parity sequence have been assigned with respect to these two levels through the measurement of DCO and iPDCO ratios of the observed γ transitions. These values have been listed in Table I.

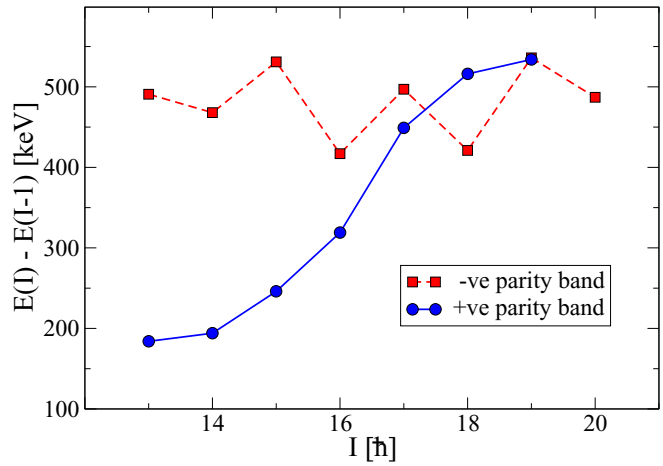

FIG. 3. The energy difference $E(I) - E(I-1)$ as a function of angular momentum for the positive and the negative-parity bands of ^{110}Ag.

It may be noted that as per the systematic of the odd-odd Ag isotopes, the lowest observed 6^+ state is common to both the positive and the negative-parity sequences. In order to realize the same structure in ^{110}Ag, a transition of 50 keV has been assumed between 7^- to 6^- levels in the negative-parity sequence, which was otherwise reported as unobserved in all the previous works [21,22]. It may be noted that this value is consistent with that of ^{106,108}Ag where these transition energies are 64.2 and 58.5 keV [1,24], respectively.

It is observed from the level scheme (Fig. 2) that the high spin levels between 12^+ and 19^+ form a band structure, which is very similar to that observed in ^{106}Ag [10]. It is interesting to note that the energies of the $M1$ transitions in this band increases smoothly in contrast to those in the negative-parity band, which exhibit a staggering in energy. This feature has been depicted in Fig. 3. The energy staggering in the negative-parity band has been associated to the signature splitting [23]. Thus, the absence of signature splitting in the positive-parity band may indicate the loss of π-rotational symmetry, which in turn can be associated to the tilted axis rotation.

In order to investigate further the underlying excitation mechanism of these states, the transition rates were measured for the $I = 15^+$ to 18^+ levels. The lifetime of these levels were obtained by fitting the observed line shapes of the corresponding $M1$ transitions at 57°, 90°, and 123° simultaneously with the theoretical line shapes derived from the code LINESHAPE by Wells and Johnson [25]. The details of the fitting procedure are given in Ref. [2]. The observed line shape of the 516 keV ($18^+ \rightarrow 17^+$) transition was fitted assuming 100% side feed. This analysis provided the effective lifetime for the $I = 18\hbar$ level. The next lower transition in the sequence was fitted with this effective lifetime and the side-feeding lifetime as the input parameters. The side feeding into each level were modeled as a cascade of five transitions with the comparable moment of inertia of the present band. The quadrupole moments of the side-feeding sequences were

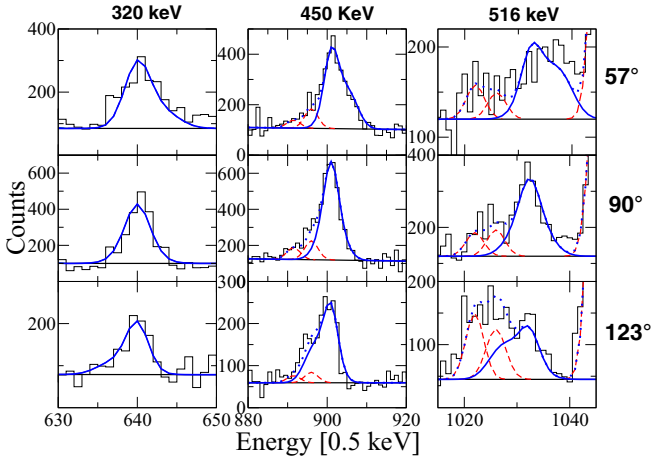

FIG. 4. Examples of the line-shape fits for 320 ($16^+ \rightarrow 15^+$) keV, 450 ($17^+ \rightarrow 16^+$) keV, and 516 ($18^+ \rightarrow 17^+$) keV transitions at 57°, 90°, and 148° with respect to the beam direction. The Doppler broadened line shapes are drawn in solid lines while the contaminant peaks are shown in dashed lines. The result of the fit to the experimental data is shown in dotted lines.

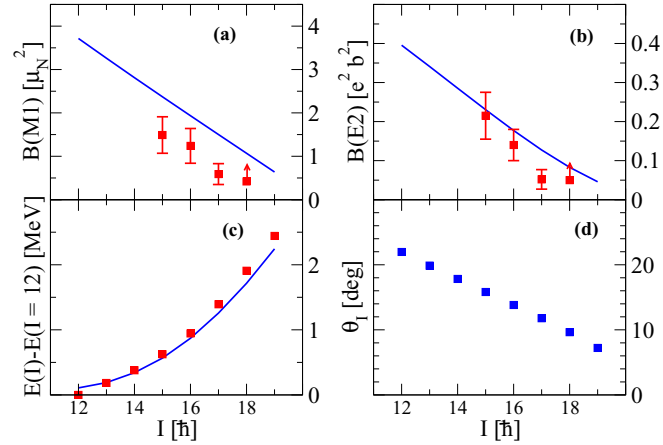

FIG. 5. The measured and calculated (a) $B(M1)$, (b) $B(E2)$ rates for the positive-parity band of ^{110}Ag. (c) The measured and the calculated Routhian $[E(I) - E(I = 12)]$, where $E(I = 12)$ is the band-head energy and the solid line represents the calculated values from SPAC. (d)The tilt angle (θ_I) as a function of angular momentum (I).

allowed to vary, which, combined with the moment of inertia, gave an effective side-feeding lifetime parameters for each level. It is to be noted that the side feeding at a given level was fixed to the missing intensity determined from the spectra at 90° with respect to the beam direction. This way the three levels of the band were added sequentially one after another and the corresponding line shapes were fitted. The uncertainties in these measurements were derived from the behavior of the χ^2 around the minimum for the simultaneous fit at the three angles. The effect of variation of the side-feeding intensity and lifetime were estimated by finding the level lifetimes for the extreme values of these two parameters and it was found to be $\sim 20\%$. The final statistical uncertainty was calculated by adding in quadrature the uncertainties due to line-shape fitting, side-feeding intensity, and side-feeding lifetime. However, this estimated error does not include the systematic uncertainty that arises due to the choice of the stopping powers, which may have additional contribution of 8% at low spins to 15% for the topmost level. The examples of the line-shape fits are shown in Fig. 4 and the measured level lifetime values are given in the level scheme of Fig. 2.

The experimentally observed level lifetimes were used to extract the electromagnetic transition rates without any loss of generality. The $B(M1)$ and $B(E2)$ rates were calculated using the following relations [26]:

$$B(M1) = 5.68 \times 10^{-14} \times {E_\gamma}^{-3} \times B_r \times \frac{1}{\tau}. \quad (1)$$

$$B(E2) = 8.156 \times 10^{-14} \times {E_\gamma}^{-5} \times \frac{(1 - B_r)}{\tau}, \quad (2)$$

where B_r is the branching ratio, τ is the mean lifetime of the excited level in seconds and the γ-ray energy (E_γ) is expressed in MeV. It is to be noted that the mixing ratio δ, was assumed to be zero while calculating the $B(M1)$ rates for all the $\Delta I = 1$ transitions. The experimentally derived $B(M1)$ and the $B(E2)$ values using the Eq. (1) and Eq. (2) have been plotted in Figs. 5(a) and 5(b), respectively. It is apparent from the Fig. 5 that both the $B(M1)$ and the $B(E2)$ rates fall rapidly between the spin range of $15\hbar$–$17\hbar$. A similar trend has already been reported in the positive-parity band in ^{106}Ag [10]. In contrast, the negative-parity levels in the same spin domain exhibit the staggering in the $B(M1)$ rates while the $B(E2)$ rates remain nearly constant [13].

IV. DISCUSSION

In ^{110}Ag, the positive-parity low spin states has been considered to arise from the $\pi g_{9/2}^{-1} \otimes \nu(d_{5/2}/g_{7/2})^1$ configuration. This assignment is due to the limited phase space available to the proton sector due to large $Z = 50$ shell gap and the presence of $h_{11/2}$ intruder orbital for the neutrons. Thus, the choice of positive-parity states at low spin, restrict the neutron single-particle levels to the $d_{5/2}$ and the $g_{7/2}$ while the proton to the $g_{9/2}$ orbital. The high spin levels ($I > 12\hbar$) have significantly large aligned angular momentum of $\sim 10\hbar$. In this mass region, such large aligned angular momentum can only be associated with the neutron alignment in $h_{11/2}$ orbital, which lead to the $\pi g_{9/2}^{-1} \otimes \nu[(d_{5/2}/g_{7/2})^1 h_{11/2}^2]$ configuration for the positive-parity band. It may be noted that this configuration is suitable for shears mechanism and, thus, the observed falling trends in the $B(M1)$ and the $B(E2)$ rates can be understood as a consequence of this mechanism.

In this context, we have calculated the experimental Routhian and the transition rates within the framework of the SPAC model to examine the validity of the above assumptions. Recently this model has been successfully used to describe the Routhian and the transition rates in both the positive- and the negative-parity bands in ^{106}Ag [9,10]. In this model, the total angular momentum $\vec{I}$, is constructed by the angular momentum vectors of the deformation ($\vec{j}_1$) and the rotation ($\vec{j}_2$) aligned valence particles and the core rotation ($\vec{R}$). However,

the tilt angle, θ_I, between the total angular momentum ($\vec{I}$) and core rotation $\vec{R}$, which is a constant of motion in the conventional shears model, changes continuously in SPAC formalism. This is the consequence of the assumption that the principal axis rotation is strong enough to keep the orientation of the rotationally aligned angular momentum vector ($\vec{j}_2$) unchanged. The details of this model can be found in Ref. [9].

The present SPAC calculation for the positive-parity band was performed for the $\pi g_{9/2}^{-1} \otimes \nu[(d_{5/2}/g_{7/2})^1 h_{11/2}^2]$ configuration with the band head at 12^+. The deformation aligned angular momentum vector ($\vec{j}_1$) was assumed to be $4.5\hbar$, which corresponded to the contribution of the lone proton hole in the $g_{9/2}$ orbital. The $\vec{j}_2$ was calculated to be $10.5\hbar$ to reproduce the band head. It is to be noted that the maximum possible angular momentum that can be generated by this geometry is $15\hbar$. However, the present band extends up to $19\hbar$ and this extra four units of angular momentum is accommodated in the present version of SPAC through the core rotation. The best simultaneous fit to the experimental Routhian and $B(M1)$ rates was observed for an effective moment of inertia $\mathcal{J} = 8\,\hbar^2/\mathrm{MeV}$ and the shears potential $V_2 = 0.8$ MeV, which are consistent with this mass region [9,10]. The results of these best fits to the $B(M1)$ transition rates and the experimental Routhian are shown by the solid lines in Figs. 5(a) and 5(c), respectively. It is to be noted that though the present calculation reproduces the trend of the observed $B(M1)$ rates, it predicts relatively higher values. This may be attributed to the simplistic geometric approach of the model calculation as well as the choice of the gyromagnetic factor to their free values. The best fit to the experimental $B(E2)$ values [Fig. 5(b)] was obtained for $eQ_{eff} = 3.5$ eb and $eQ_{coll} = 0.5$ eb. It is to be noted that eQ_{eff} is related to the core polarization effect measured by the polarization charge e_{pol} [12]. In the present case a polarization charge of $e_{pol} \sim 2e$ is obtained, which is consistent for the present single-particle configuration [10] of one valance proton. The variation of the tilt angle (θ_I) as a function of the angular momentum is shown in Fig. 5(d). This value changes from 22° at $I = 12\hbar$ to 7° at $I = 19\hbar$ while in the present geometry, the principal axis rotation corresponds to $\theta_I = 0°$.

From the above discussion it can be concluded that the observed features of the positive-parity band can be described by assuming nonprincipal (tilted) axis rotation. While, the properties of the negative-parity band have been described by assuming principal axis rotation [13]. Thus, in the same spin range of $I = 13$ to $19\hbar$, there is a coexistence of the principal axis and the tilted axis rotation in ^{110}Ag. This is a unique observation for $A \sim 100$ region.

V. SUMMARY

In summary, the positive-parity band structure of ^{110}Ag has been identified for the first time. The observed levels form a band structure above $I = 12^+$ where the energy of the $M1$ transitions increases with increasing spin. The levels lifetimes in this band has been measured and the deduced $B(M1)$ and $B(E2)$ rates exhibit a falling trend with increasing spin. These are the distinctive features of tilted axis rotation. On the other hand, the observed staggering in the $M1$ energy and $B(M1)$ rates in the negative-parity band are the distinctive features of principal axis rotation. Thus, there is a coexistence of the principal and the tilted axis rotation in the same spin domain of ^{110}Ag.

ACKNOWLEDGMENTS

The authors would like to thank all the technical staff of the Pelletron facility at IUAC, New Delhi, for smooth operation of the machine. This work was partly funded by the Department of Science and Technology, Government of India (No. IR/S2/PF-03/2003-I). In addition, B.D. would like to thank SINP for providing research support and P.D. acknowledges the support of University Grants Commission, India, through Grant No. PSW-058/15-16(ERO).

[1] J. Sethi *et al.*, Phys. Lett. B **725**, 85 (2013).
[2] N. Rather *et al.*, Phys. Rev. Lett. **112**, 202503 (2014).
[3] E. O. Lieder *et al.*, Phys. Rev. Lett. **112**, 202502 (2014).
[4] P. Joshi, M. P. Carpenter, D. B. Fossan, T. Koike, E. S. Paul, G. Rainovski, K. Starosta, C. Vaman, and R. Wadsworth, Phys. Rev. Lett. **98**, 102501 (2007).
[5] R. M. Clark *et al.*, Phys. Rev. Lett. **82**, 3220 (1999); D. G. Jenkins *et al.*, Phys. Lett. B **428**, 23 (1998); C. J. Chiara, D. B. Fossan, V. P. Janzen, T. Koike, D. R. LaFosse, G. J. Lane, S. M. Mullins, E. S. Paul, D. C. Radford, H. Schnare, J. M. Sears, J. F. Smith, K. Starosta, P. Vaska, R. Wadsworth, D. Ward, and S. Frauendorf, Phys. Rev. C **64**, 054314 (2001).
[6] S. Frauendorf, Rev. Mod. Phy. **73**, 463 (2001).
[7] P. Datta, S. Chattopadhyay, P. Banerjee, S. Bhattacharya, B. Dasmahapatra, T. K. Ghosh, A. Goswami, S. Pal, M. S. Sarkar, S. Sen, H. C. Jain, P. K. Joshi, and Amita, Phys. Rev. C **69**, 044317 (2004).
[8] P. Datta, S. Roy, S. Pal, S. Chattopadhyay, S. Bhattacharya, A. Goswami, M. SahaSarkar, J. A. Sheikh, Y. Sun, P. V. MadhusudhanaRao, R. K. Bhowmik, R. Kumar, N. Madhavan, S. Muralithar, R. P. Singh, H. C. Jain, P. K. Joshi, and Amita, Phys. Rev. C **78**, 021306(R) (2008).
[9] B. Das *et al.*, Phys. Rev. C **93**, 064322 (2016).
[10] B. Das *et al.*, Phys. Rev. C **95**, 051301(R) (2017).
[11] R. M. Clark and A. O. Macchiavelli, Annu. Rev. Nucl. Part. Sci. **50**, 1 (2000).
[12] E. O. Podsvirova *et al.*, Eur. Phys. J. A **21**, 1 (2004); A. A. Pasternak *et al.*, *ibid.* **23**, 191 (2005); **37**, 279 (2008); A. A. Pasternak, E. O. Lieder, and R. M. Lieder, Acta Phys. Pol. B **40**, 647 (2009); S. Rajbanshi *et al.*, Phys. Rev. C **89**, 014315 (2014).
[13] S. Roy *et al.*, Phys. Lett. B **710**, 587 (2012).
[14] S. Muralithar *et al.*, Nucl. Instrum. Methods Phys. Res., Sect. A **622**, 281 (2010).
[15] R. K. Bhowmik, A. K. Jain, and D. C. Biswas, Proceedings of the DAE Symposium on Nuclear Physics **44B**, 422 (2001).
[16] S. Das, S. Samanta, S. Chatterjee, A. Ghosh, R. Bhattacharjee, R. Raut, S. S. Ghugre, and A. K. Sinha, Proceedings of the DAE Symposium on Nuclear Physics **62**, 1066 (2017).

[17] D. C. Radford, Nucl. Instrum. Meth. Phys. Res. A **361**, 297 (1995).
[18] A. Krämer-Flecken *et al.*, Nucl. Instr. and Meth. Phys. Res. A **275**, 333 (1989).
[19] K. Starosta *et al.*, Nucl. Instr. and Meth. Phys. Res. A **423**, 16 (1999).
[20] G. Gürdal and F. G. Kondev, Nuclear Data Sheets **113**, 1315 (2012).
[21] M.-G. Porquet *et al.*, Eur. Phys. J. A **15**, 463 (2002).
[22] H. Xin *et al.*, Chin. Phys. C **32**, 143 (2008).
[23] I. Hamamoto, Phys. Lett. B **235**, 221 (1990).
[24] D. Jerrestam *et al.*, Nucl. Phys. A **577**, 786 (1994).
[25] J. C. Wells and N. R. Johnson, Oak Ridge National Laboratory Report No. ORNL-6689, 1991.
[26] T. K. Alexander *et al.*, *Advances In Nuclear Physics*, Vol. 10 (Springer Science+Business Media, New York, 1978).